

# Additive Manufacturing of Recycled Composites



Andrea Mantelli , Alessia Romani , Raffaella Suriano ,  
Marinella Levi , and Stefano Turri 

**Abstract** An additive remanufacturing process for mechanically recycled glass fibers and thermally recycled carbon fibers was developed. The main purpose was to demonstrate the feasibility of an additive remanufacturing process starting from recycled glass and carbon fibers to obtain a new photo- and thermally-curable composite. 3D printable and UV-curable inks were developed and characterized for new ad-hoc UV-assisted 3D printing apparatus. Rheological behavior was investigated and optimized considering the 3D printing process, the recycle content, and the level of dispersion in the matrix. Some requirements for the new formulations were defined. Moreover, new printing apparatuses were designed and modified to improve the remanufacturing process. Different models and geometries were defined with different printable ink formulations to test material mechanical properties and overall process quality on the final pieces. To sum up, 3D printable inks with different percentages of recycled glass fiber and carbon fiber reinforced polymers were successfully 3D printed.

**Keywords** 3D printing · Rheology · Glass fiber · Carbon fiber · Mechanical properties · Composites

## 1 Introduction to Composites Additive Re-Manufacturing: Challenges and Objectives

Over the last years, additive manufacturing (AM) has been emerging as a valid technology for the cost-effective realization of complex and customized components made of polymer composites through a layer-by-layer process [1, 2]. However, AM

---

A. Mantelli (✉) · A. Romani · R. Suriano · M. Levi · S. Turri  
Department of Chemistry, Materials and Chemical Engineering “Giulio Natta”, Politecnico Di Milano, Piazza Leonardo da Vinci 32, 20133 Milano, Italy  
e-mail: [andrea.mantelli@polimi.it](mailto:andrea.mantelli@polimi.it)

A. Romani  
Department of Design, Politecnico Di Milano, Via Durando 38/A, 20158 Milano, Italy

© The Author(s) 2022  
M. Colledani and S. Turri (eds.), *Systemic Circular Economy Solutions for Fiber Reinforced Composites*, Digital Innovations in Architecture, Engineering and Construction, [https://doi.org/10.1007/978-3-031-22352-5\\_8](https://doi.org/10.1007/978-3-031-22352-5_8)

of composites shows some weaknesses such as the optimization of the processability, which changes according to the materials, and the resulting properties associated with the adhesion between layers as well as between matrices and reinforcing fillers [3, 4]. If recycled fibers are used as a reinforcement, the availability of composite wastes with different compositions and geometries, and the resulting variability of the filler properties, introduce other variables to be governed into the process. Therefore, it is necessary to validate the opportunity to develop an additive remanufacturing process of composites reinforced with recycled glass fibers (GFs) and carbon fibers (CFs). This requires the development of new 3D printable composite inks together with a new custom-made 3D printing system to obtain a good flowability of inks during the extrusion and high shape retention after the extrusion through the nozzle.

For this purpose, the aim of this study was firstly to characterize recycled fibers in terms of diameter sizes and dimension distributions. Secondly, different formulations of 3D printable inks were investigated by starting from a UV-curable acrylic resin combined with different amounts of recycled glass fiber reinforced polymers (rGFRP) and carbon fiber reinforced polymer (rCFRP). Rheological properties of inks were studied and optimized considering various recycled fiber percentages and mixing technologies. This led to the definition of a few requirements for 3D printable ink compositions. Moreover, a set-up for the 3D printing apparatus coupled with a UV-light to crosslink UV-curable ink was built up for these new 3D printable inks. Post-curing treatments after the 3D printing process enabled to maximize the crosslinking degree of 3D printed materials and their final mechanical properties. Various 3D structures and components were also 3D printed to validate the feasibility of the additive remanufacturing process with the reuse of end-of-life (EoL) composites.

## **2 Additive Manufacturing of Composites State of the Art**

### ***2.1 Commercial Solutions***

3D printing of polymers is spreading fast in the field of automotive industries, particularly in many different brands of sports and standard cars. Sports car brands are currently developing the AM technology to improve their production process since it allows the fabrication of very complex geometries and, in some cases, reduces sensibly the production time and costs.

In 2014, Local Motors presented, for the first time, a car completely 3D printed by fused deposition modeling (FDM) technology and composed of acrylonitrile butadiene styrene polymer (ABS) reinforced with carbon fibers [5]. Since 2017, McLaren Formula 1 team has been using AM to produce race-ready parts of the car and tooling for immediate evaluation during practical sessions that need specific features not achievable with traditional manufacturing methods [6]. For instance, the material used to produce a structural bracket was a thermoplastic polyamide

reinforced with chopped carbon fibers (FDM® Nylon 12CF), and the component was obtained in just 4 h instead of 2 weeks, which were necessary for standard processes.

Very recently, Moi composites s.r.l produced the world's first 3D printed real boat in continuous fiberglass thermoset material called MAMBO (Motor Additive Manufacturing Boat) with a patented additive manufacturing process [7]. Another example of AM technology currently used for the 3D printing of long fiber reinforced composite 3D printing is the continuous fiber printer developed by MarkForged® [8]. For instance, this printer and technology were deployed for the prototyping of fins for surfboards, showing a high level of mechanical strength when they were 3D printed with a thermoplastic filament of polyetherimide (ULTEM) reinforced with carbon fibers [9].

## 2.2 Academic Advancements

Over the last decade, many academic researchers have investigated and employed the FDM technology for the additive manufacturing of short fiber reinforced composites consisted of thermoplastic matrices and different types of reinforcements [10, 11]. The most common thermoplastic materials used as matrices are polylactic acid (PLA), ABS, polycarbonate (PC), nylon, and polyether ether ketone (PEEK), which seemed to provide some advantages such as a higher tensile strength compared to the other 3D printed thermoplastic polymers [12–14]. Regarding the reinforcement, natural fibers, which are for example made of hemp and wood have been applied and tested for the AM of polymer composites [15, 16]. However, synthetic fibers, i.e. short GFs as well as short and long CFs, are the most widespread reinforcing fillers added in the 3D printing of thermoplastics polymers [4, 17].

Another 3D printing technology used for the additive manufacturing of composites is liquid deposition modeling (LDM), based on the extrusion of liquid or viscous inks that can solidify just after the extrusion through the nozzle. A strategy commonly employed to induce a fast solidification is the application of heat and/or UV light that can trigger the polymerization of ink components using a UV and thermal initiators. In 2014, Compton and Lewis developed the LDM process, also called direct ink writing (DIW), capable of extruding short carbon fiber epoxy-based composites [18]. After the 3D printing of the composite structures, a thermal curing cycle was needed to completely solidify the resin. This study evidenced how the high aspect ratio fibers were aligned in the direction of the print during the process, conferring to the material the behavior of a classical composite. In 2017, the same authors prosecuted their previous study focusing on the orientation of the fibers in the desired orientation [19]. They developed and used a rotating printing head capable of imparting a particular “rope-like” orientation to the printed fibers, leading to a material with great performances in both compression and impact. The production of 3D printed carbon fiber composites was also attempted by Mahajan and Cormier with the aim of fabricating an oriented short carbon fiber epoxy composite [20]. A similar approach

was used to 3D print CFRPs with orthotropic physical properties [21]. Even in this study, the ink material used in the DIW process exhibited a shear-thinning behavior with a moderate yield stress, which was necessary to allow the 3D printing and show excellent shape retention after the deposition to maintain the printed geometry. A thermally cured aromatic thermoset resin system with latent thermal cure catalysis was developed to induce the generation of a strong Lewis acid above  $\sim 70$  °C and initiate a thermally activated cationic self-crosslinking among the epoxide functionalities of the resin. The formulated resin can remain stable at 20 °C for over 5 days at catalyst concentrations below 2% by weight and the gelation of the system and curing to full network density can be achieved in less than 5 s when the applied temperatures reach 150–200 °C.

Another study was also focused on the 3D printing of carbon fiber and glass fiber reinforced thermosetting resins with a standard desktop 3D printer modified for the LDM deposition [22]. In this study, a novel setup of an extrusion-based printer coupled with UV-light sources was employed to print a batch of specimens reinforced both with glass fibers and carbon fibers (up to 30wt%). Moreover, an interpenetrating polymer network (IPN) resin system was used in the UV-assisted 3D printing of composites. The formulated IPN system was composed of a thermal activated epoxy resin and a UV-curable acrylic resin. The resin system undergoes two sequential curing mechanisms: the former was due to the UV-curing of the acrylic resin during the extrusion process and the latter increased the crosslinking degree of the 3D printed enhanced mechanical properties. The enhanced stiffness and mechanical resistance of the glass/carbon fiber reinforced IPN resin systems were also demonstrated in another paper [23]. The mechanical properties of GFRP and CFRP systems exhibit an average increase in elastic modulus of 37% and 44%, respectively, compared to unfilled blends and a tensile strength increase of 19% and 91%.

Recently, 3D printed structures obtained with continuous carbon fiber reinforced PLA filaments were recycled and reused to produce the raw material for a subsequent 3D printing process [24]. The reuse of mechanically recycled EoL GFRPs as a reinforcement for the 3D printing of composites was very recently achieved [25]. The 3D printed composites with mechanically recycled GFs showed results comparable to 3D printed composites filled with virgin GFs, thus fostering the implementation of a circular economy case for thermoset composites [26].

### 3 UV-Assisted Additive Manufacturing

#### 3.1 Working Principle

As depicted in Fig. 1 the process starts with the 3D printable ink preparation, then the UV curable ink is extruded from a syringe and a UV light-emitting diodes (LEDs) apparatus is switched on during ink deposition. As soon as the ink flows out from

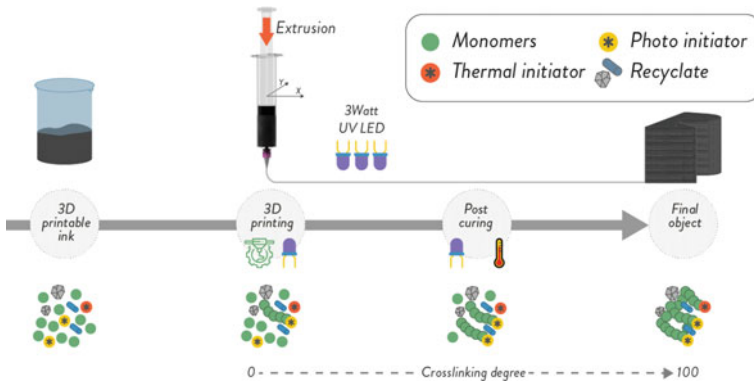


**Fig. 1** UV-assisted liquid deposition modeling process description

the syringe nozzle it starts to cure. The free-radical photo-crosslinking process is normally fast enough to assure the layer-by-layer build-up process.

### 3.2 Machine Modifications

At the time of this work, a commercial UV-assisted 3D printer capable of processing composite inks was not available. For this reason, an open-source 3D printer was modified as follows.

The first modifications of the 3Drag printer (version 1.2, Futura Elettronica, Italy) were developed in previous work [22]. It is an open-source cartesian desktop-size 3D printer with a Z-head mechanical arrangement, meaning that the X and Y axis movements are delegated to the plate, while the tiny Z-axis movements are left to the head. This arrangement is very favorable in the case of bigger and heavier extruders since the limited accelerations do not cause any inertia-related issues. The main changes were done by modifying the extruder as shown in Fig. 2: the standard system was completely removed, and a custom extruder was installed in its place [27]. The custom system transfers the rotation of a stepper motor to the linear motion of a syringe piston to extrude the inks. Due to the difference in the material feed system, the motor steps per mm of feedstock had to be modified in the firmware matching the actual value. This and other modifications to the firmware were needed to allow the extrusion at ambient temperature [28].

Considering the UV source, three UV-LEDs were used (395 nm, 3 W) powered by a dimmable electronic power supply [29]. Three fans cool the LEDs, extending their lifetime, maintaining constant power, controlling the heat-up, and preventing damage to their supports. A relay, connected to the fan port of the 3D printer, could be used to controls the UV source. Therefore, by switching on and off the fan port through the Gcode it is possible to directly control the LEDs. Figure 3 shows two

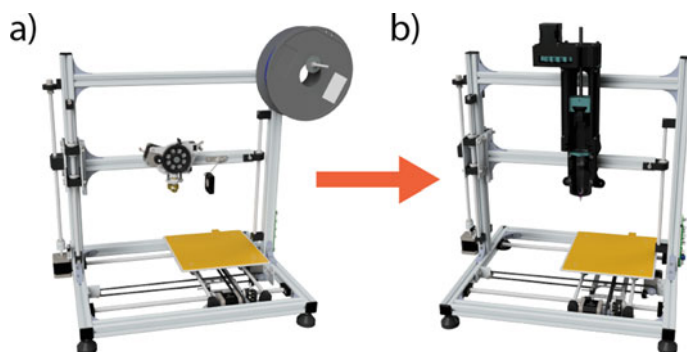


**Fig. 2** Modified 3Drag with custom extrusion head: **a** commercial 3Drag version 1.2, **b** modified 3Drag with custom extrusion head

different configurations of the UV-LEDs apparatus. The first one has the three LEDs arranged in a circle around the nozzle, pointing at its tip. The second layout has the LEDs positioned alongside the extrusion head. In this way, the polymerization of the resin can be activated after the deposition of the material. Different examples of this approach can be found in the literature [30, 31]. A physical division of the extrusion step from the resin activation step is crucial to prevent nozzle clogging or for particular situations in which the polymerization may take a longer time than the layer deposition time.

Finally, the nozzle plays a vital role in the material deposition process for LDM systems. Generally speaking, conical nozzles proved to be a better alternative to cylindrical ones, due to their geometry that reduces backpressure build-up. So, this allows for a more constant flow, less clogging, and a generally more precise extrusion [33–35]. A fundamental constraint on nozzle selection was linked to UV-shielding. To prevent the polymerization of the ink inside the nozzle, metal nozzles have to be preferred.



**Fig. 3** UV source apparatus: **a** standard configuration with LEDs pointing at the nozzle tip, **b** side configuration with LEDs pointing to the build plate alongside the extruder head [32]

### 3.3 *In-Situ Polymerization Challenges and Opportunities*

The challenges related to the material crosslink itself during the manufacturing process are mainly related to the rapidity of the process and its activation. Among the processes suitable for rapid crosslinking, radical photo-crosslinking is the most promising. These systems can provide a set time of seconds, or fractions of seconds, allowing to build the 3D object layer by layer. Examples can be found in literature where a self-standing ink is crosslinked after the 3D object manufacturing [18, 36]. The opportunities of the in-situ polymerization are both to use simpler ink systems that do not need to be self-sustaining or to have the possibility of crosslinking part of the 3D object to build bigger and more complex structures [25].

## 4 Experimental Methods, Materials Description, and Requirements

To better understand and follow the results that will be presented in the next chapter, the experimental methods, and the materials used will be described. The workflow followed in the development of the research can be divided into five interconnected steps: recyclete characterization, ink formulation, curing cycle, process development, material characterization. Figure 4 shows a flow chart that depicts the connection between the five steps and the characterization methods.

Optical microscopy and scanning electron microscopy (SEM) were performed respectively with Olympus BX60 (Olympus Corp., Japan) and Cambridge Stereoscan 360 (Cambridge Instrument Company Ltd., UK). Recyclate fibers were analyzed with a particle analyzer software [37]. Thermogravimetric Analyses (TGA) were

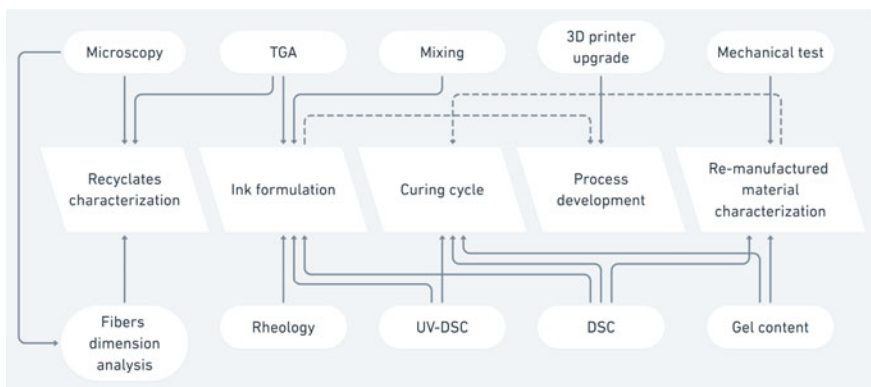


**Fig. 4** A Flow chart representing the tests performed for the development of the remanufacturing process and the 3D printable inks

performed on TA INSTRUMENTS Q500 TGA (TA Instruments, Inc, US). Rheological tests were performed with Kinexus DSR (Malvern Panalytical Ltd., UK) and Discovery HR-2 (TA Instruments, Inc, US). Differential scanning calorimetry (DSC) was performed with a Mettler–Toledo DSC/823e (Mettler Toledo, USA) equipped with Lightningcure LC8 (Hamamatsu Photonics, Japan) for UV-DSC. Tensile tests were performed with Zwick Roell Z010 (ZwickRoell GmbH & Co. KG, Germany). Detailed descriptions of the methodologies were described in previous works [25, 26].

#### **4.1 Materials Description**

3D Printable inks were mainly composed of a photo and thermo-curable acrylic-based resin matrix and recycled GFRP or CF reinforcement, mixed in different percentages. The matrix consisted of the ethoxylate bisphenol A diacrylate resin (hereinafter named SR349), purchased from Arkema and locally distributed by Came S.r.l., Italy. Butanediol dimethacrylate (hereinafter called BDDMA) and BYK-7411 ES (hereinafter called BYK) were added in different proportion as a reactive diluent and as a rheological modifier respectively, both purchased from Sigma-Aldrich, Italy; Dicumyl peroxide (Sigma-Aldrich, Italy) and Ethyl phenyl(2,4,6-trimethylbenzoyl) phosphinate (hereinafter named TPO-L, purchased from Lambson Limited, UK) were added at the fixed proportion of 0.3%wt and 3%wt as thermal activator and as photo activator respectively.

Recycled GF powders can be divided into two main groups: Rivasca GFRPs (RIV) and Gamesa GFRPs (GAM). RIV GFRPs originally consisted of scraps of a styrene-based unsaturated polyester resin reinforced with 5 cm long glass fibers with a diameter of 13  $\mu\text{m}$  (supplied by Rivasca S.p.A., Italy). GAM GFRPs derive from Siemens Gamesa Renewable Energy S.A. End-of-Life (EoL) wind turbines, and they were made of an epoxy resin reinforced by continuous GF. Successively, they were shredded and supplied from Consiglio Nazionale di Ricerca—Sistemi e Tecnologie Industriali Intelligenti per il Manifatturiero Avanzato (Stiima-CNR), Italy, please refers to Chap. 4 of the book for detail of the shredding process. Recycled CFs were provided by Stiima-CNR after shredding with a cutting mill by Retsch GmbH (model SM-300, Haan, Germany): they were previously pyrolyzed by Tecnalia (TEC) from Aernnova (AER) expired prepreg. After the pyrolysis, a sizing material was applied by Tampere University of Technology (TUT) as described in Chap. 7 of the book. Finally, a cryogenic shredding was performed with a quad blade chopper CH580 (Kenwood Limited, Havant, United Kingdom) and the powder was sieved manually with a 100  $\mu\text{m}$  sieve.



## 4.2 Additive Remanufacturing Requirements

**Recyclate particle dimensions.** Many works related to clogging mechanisms of spherical particle-filled liquids have been published [38–40]. In particular, the nozzle and particle diameter can be related to defining a maximum particle diameter to prevent clogging [41]:

$$D/d > 6.2 \quad (1)$$

where  $D$  is the nozzle diameter and  $d$  the particle diameter. Dealing with fibers literature shows their alignment to the flow under extrusion [18]. Nevertheless, sudden restriction of the channel and small nozzle diameter can cause their blocking and, consequently, the clogging of the nozzle. Tentatively, Eq. (1) can be used to define a maximum length of the fibers, substituting  $d$  with  $l$ : considering a nozzle of 1 mm in diameter, the corresponding value is 160  $\mu\text{m}$ .

**Ink rheology.** This material property is limited by the process and the maximum pressure supported by the extrusion system. The extrusion head described before works by applying a force to the syringe's piston which generates pressure inside the syringe. Overloading a stepper motor will not compromise the motor necessarily. However, the motor will not rotate. The most used model in literature links the power law rheological model with the maximum pressure or force exerted by the extrusion system. Starting from the derivation made for a commercial FDM extruder [41], it is possible to express the maximum viscosity in function of the maximum pressure exerted by the extrusion head:

$$\eta < \frac{\pi \cdot c \cdot P_0 \cdot d^4 \cdot n}{32Q \cdot l \cdot (3n + 1)} \quad (2)$$

where  $c$  is the ratio between the pressure drop inside the last section of the nozzle and the total pressure drop inside the syringe,  $P_0$  is the maximum pressure sustained by the extrusion system,  $d$  is the nozzle diameter,  $n$  is the flow behavior index,  $Q$  is the ink volumetric flow and  $l$  is the length of the last section of the nozzle. Different from the derivations found in a previous work [41], Eq. (2) does not make the approximation of Newtonian flow and express the viscosity in function of the volumetric flow rate instead of the printing velocity, which is more suitable for the LDM process. More information about the derivation of Eq. (2) has been extensively described in previous work [42].

**Ink reactivity.** The importance of the crosslinking kinetics has been yet described in a previous work [25]. The deposition of a layer of material over the previous one relies on the stability of the deposited material.

Rheological modifiers are eventually used to produce inks with suitable yield stress [18, 36]. A drawback of this solution is the height limit of the 3D printed object since the weight of the object itself can exceed the yield stress, causing the structure to collapse [43]. Photo-crosslinking was set as a requirement for 3D printable inks,

**Table 1** Recyclate properties

Recyclate name	RIV ultrafine	GAM fine	AER fine
Short name	RIVUF	GAMF	AERF
Recycling method	Mechanical	Mechanical	Thermal/Mechanical
Nominal granulometry [ $\mu\text{m}$ ]	$3.5 \pm 4.2$	80	100
rGF/rCF content [%wt.] by TGA	$12 \pm 1$	$70 \pm 0.5$	100
rGF/rCF average length [ $\mu\text{m}$ ]	$102.8 \pm 33.5^1$	$34.4 \pm 47.7$	$74.6 \pm 48.3$
rGF/rCF average diameter [ $\mu\text{m}$ ]	$9.4 \pm 4.31$	$13.5 \pm 6.0$	6.5
rGF/rCF average aspect ratio (l/d)	$11.4 \pm 1.71$	$2.3 \pm 3.2$	$11.5 \pm 7.4$

to take advantage of 3D printing freedom. Contemporarily, big volume models can be fabricated without maximum dimensions limits, because the material will rapidly crosslink and the shape set.

## 5 Results and Validation: Material Characterization and Remanufacturing Description

As previously described the material development is crucial to fully exploit the potentiality of 3D printing technology. This section will be focused on the development of the 3D printable inks, the process optimization, and the material properties.

### 5.1 Recyclate Characterization

Recyclates' characteristics are intrinsically variable and their characterization is important in order to control the development of 3D printable inks.

Considering mechanically recycled fiber-reinforced composites, both granulometry of the recyclate and length and diameters of the fibers have been evaluated. Table 1 shows the morphological, compositional, and physical characteristics of the recyclates. RIV recyclate granulometry was measured by optical image analysis as described in a previous work [25]. For the other recyclate, the sieve size was considered. The average length and diameter of the recycled fibers were evaluated by SEM micrographs analysis performed with a specifically designed MATLAB application [37]. Figure 5. shows a sample micrograph of each recyclate.

<sup>1</sup> A low number of fibers were detected during the microscopy analysis.

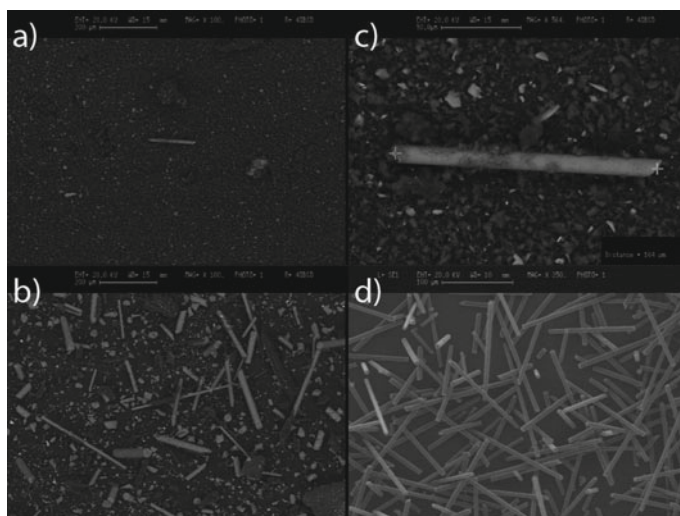


**Fig. 5** SEM micrographs of recycled composites: **a** RIFUF recyclate, **b** rGF inside RIVUF recyclate, **c** GAMF recyclate, **d** AERF recyclate

## 5.2 3D Printable Inks Formulation and Mixing

To better understand and simplify the dissertation, inks containing RIVUF and GAMF recycled composites will be named with the following nomenclature: XDYR, where X is the wt% of reactive diluent BDDMA (D), Y is the wt% of recycled composite, and R will be substituted by the short name of the recycled composites as reported in Table 1. Inks containing AERF recycled composite will be named with the following nomenclature: XBYAERF, where X is the wt% of BYK (B) and Y is the wt% of AERF recycled composite.

Considering RIVUF and GAMF recycled composites, their formulation was extensively studied, by changing the proportion between BDDMA, SR349, and recycled composites, in order to define boundaries in terms of mixing technology and recycled composite content. As depicted in Fig. 6 the use of a reactive diluent does not have a significant influence on the recycled composite content limit. Concerning mixing technology, high-velocity impeller mixers work best with material with a viscosity lower than 10 Pa·s. With high viscosity material, it is possible the creation of isolated cavities in the vessel where the material is not mixed. Double arm kneading mixers use viscous forces instead of turbulence to mix, and no isolated cavities are created [44]. Experimentally a limit in the use of a high-velocity impeller mixer was found as shown in Fig. 6.

A second rheological modifier was used in combination with the rCF. As will be discussed later, the UV conversion of AERF inks is low. It was proven that the addition of 6 wt% of BYK to the resin was enough to create hydrogen bonding structures as confirmed by rheological analysis.

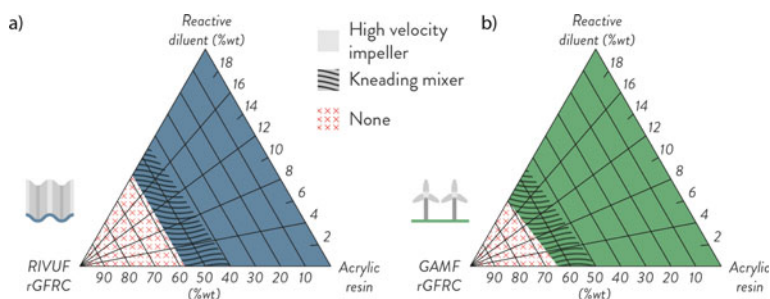


**Fig. 6** Compositional graph for RIVUF and GAMF recyclate ink formulation

### 5.3 Reactivity Measurements on the 3D Printable Inks

The reactivity of the 3D printable inks has been studied through the measurements of the enthalpy of the reaction. More in detail, the enthalpy was measured employing both DSC and photo-DSC. The latter method was used to investigate the UV conversion of the 3D printable inks and 3D printed samples. DSC was used to verify the thermal reactivity of the 3D printed samples and to measure the glass transition temperatures of the different materials at the end of the curing cycle.

Firstly, UV reactivity was studied. Figure 7 shows that increasing the recyclate content a decrease in UV conversion compared to the neat resin was obtained. Moreover, Fig. 7b shows the presence of a residual UV conversion after the manufacturing process. As a consequence, UV post-curing was performed to complete the photo-crosslinking process. As expected AERF ink shows a low UV conversion. The presence of black carbon fibers competes in the absorption of the UV radiation. Consequently, a lower amount of photo-initiator is activated. The problem was solved by adding a rheological modifier to the ink as described in Sect. 5.4 of this chapter.

After the thermal post-curing, the glass transition temperature ( $T_g$ ) was measured and gel content evaluation was performed. As reported in Table 2 AERF sample

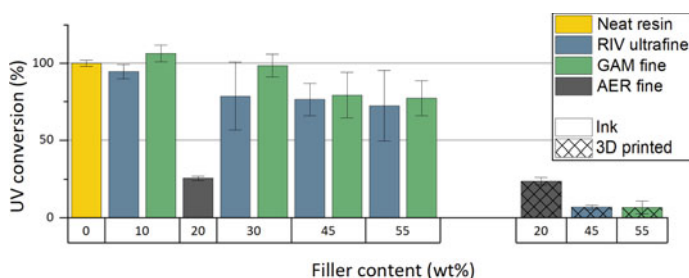


**Fig. 7** UV conversion of 3D printable inks (a) compared to the neat resin and UV conversion of 3D printed samples (b)

**Table 2** Glass transition temperature and gel content for three remanufactured materials

Material	Glass transition temperature [°C]	Gel content [%]
20D45RIVUF	110	94
0D55GAMF	100	99.4
6B20AERF	82	99

exhibit a lower  $T_g$  compared to all other remanufactured samples. Nevertheless, the gel content confirmed that a high level of crosslinking was achieved. The lower value obtained for the RIVUF sample can be related to the presence of unreacted monomers of the recycle material. More information about the post-curing process and monitoring of crosslinking were described in previous works [25, 26].

#### 5.4 Printability and Rheological Modification

A systematic rheological characterization has been performed for the different recycle formulations. The rheological behavior can be used to predict which formulation can be suitable for the particular 3D printing process used in this work. Nevertheless, the following study can be used both as a benchmark for future works with different 3D printing processes and as a guideline for determining the printability of inks via LDM process.

**RIVUF inks.** Independently from the recycle and reactive diluent content, the behavior of the material is pseudoplastic. As shown in Fig. 8, a quasi-Newtonian behavior was shown by all the formulations at a lower shear rate. By increasing the content of recycles, the range in which the materials show quasi-Newtonian behavior shifts towards higher viscosity and lower shear rate. On the other side, by increasing the reactive diluent content, the quasi-Newtonian behavior shifts towards lower viscosity and higher shear rate. The effect of shelf-time on the viscosity of already prepared formulations was investigated. As shown in Fig. 8d, the ink has a thixotropic characteristic. Therefore, its behavior change through time. Nevertheless, after 72 h the remixed ink recovers the original rheological behavior and could be processed in the same condition as after the ink preparation. Comparing the rheological behavior of Fig. 8 to the maximum viscosity model of Eq. (2), inks containing 55 wt% of RIVUF recycle cannot be extruded by the extruder used in this work.

**GAMF inks.** As done for RIVUF inks, the flow ramp test on GAMF inks has shown a pseudoplastic behavior with a flow behavior index change (Fig. 9). The behavior at the higher shear rate is constant for inks with up to 60 wt% of recycle. The addition of the reactive diluent decreases the overall viscosity, which is similar to what was expected from the RIVUF rheology study. However, the lower viscosity and the overall bigger particle of GAMF recycle, respect to RIVUF recycle, evidenced a problem of separation of the recycle particles from the resin. The

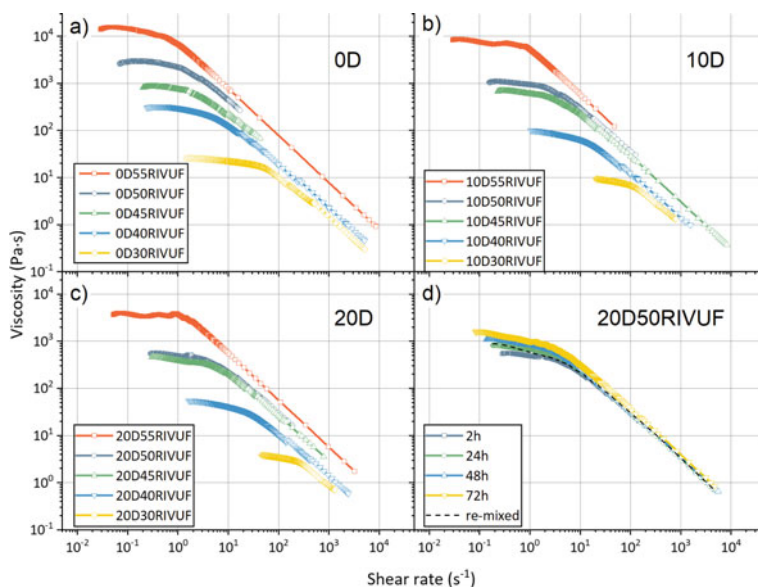


**Fig. 8** Flow ramp test for RIVUF recyclate inks: **a** tests on RIVUF inks without reactive diluent, **b** tests on RIVUF inks containing 10 wt% of reactive diluent, **c** tests on RIVUF inks containing 20 wt% of reactive diluent, **d** effect of shelf-time and re-mixing on the viscosity of 20D50RIVUF ink

behavior of GAMF inks without the presence of BDDMA was furtherly studied. As shown in Fig. 9c–d, the viscosity at lower shear rates is different if the pre-shear was not applied or was applied. Consequently, the ink behavior before the loading into the syringe will be different from that after the loading. Moreover, this difference highlights the thixotropic characteristic of the inks' rheological behavior. Considering Fig. 9a–b and calculation performed with Eq. (2), only the inks with 65 wt% of GAMF recyclate will not be suitable for the extrusion process considered.

**AERF inks.** The addition of BYK additive can introduce in the material a rapid recovery of the deformation, and it induces a rapid fluid/solid-like transition thanks to the formation of hydrogen bonding structure [45]. A three-step strain test has been developed to simulate the 3D printing process steps and measure the response of the material before, during, and after the extrusion. The graph in Fig. 10 shows the strain stimulus applied and the responses of different inks. The rest properties of the material are recorded in the first and third step where a strain very close to zero was applied. In the second step, a strain is applied to simulate the extrusion of the material.

The addition of BYK additive is not enough to assure a rapid fluid/solid-like behavior transition. In order to exhibit a rapid recovery, a minimum of 20 wt% of rCF has to be added to the formulation.

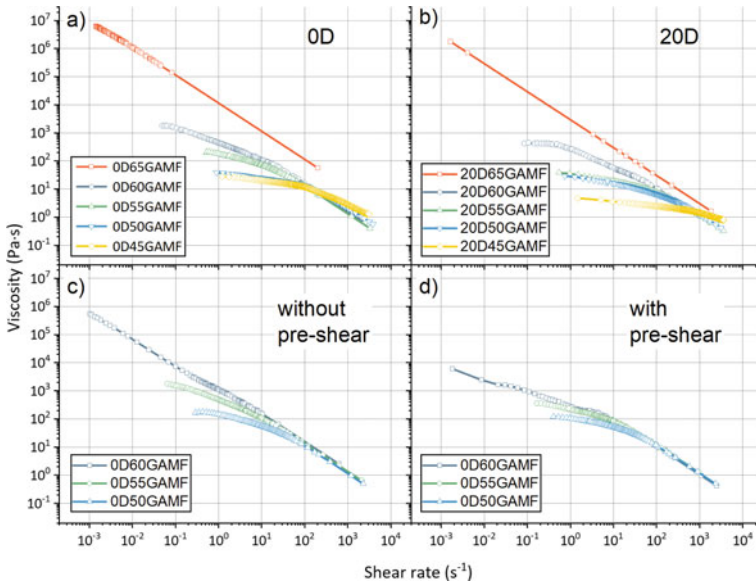


**Fig. 9** Flow ramp test for GAMF recyclate inks: **a** tests on GAMF ink without reactive diluent, **b** tests on GAMF ink containing 20 wt% of reactive diluent, **c** tests on GAMF ink performed without the pre-shear step, **d** tests on GAMF ink performed with the pre-shear step

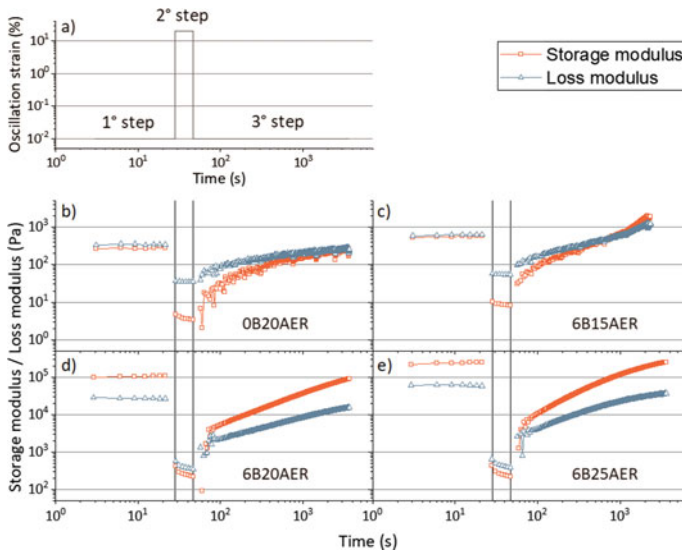


**Fig. 10** Three-step strain tests on different AERF ink formulations

## 5.5 Additive Remanufacturing Process and Surface Finishing

As discussed before, 3D printable ink could be improved by modifying recyclate content and/or by adding rheological modifiers. For these reasons, 3D printing parameters optimization is connected to the development of the inks. Starting from the consideration about reactivity and rheological behavior discussed before, one ink for each recyclate has been selected and their process parameters are reported in Table 3.

Differences between inks developed from different recyclates are not only related to process parameters and composition but also on appearance: for instance, RIVUF 3D printed objects have a more visible layer-by-layer regular appearance (Fig. 11), while random textured appearance is exhibited by GAMF 3D printed samples (Fig. 12). Furthermore, AERF pieces show similarities with GAM ones, since layer-by-layer surface finishing is less noticeable (Fig. 13). These big differences can affect 3D printable ink applications and product perception for users.

As shown in Fig. 12e, f the arch model 3D printing exploits the use of UV-assisted LDM process by enabling the deposition of overhang structures. Promising results have been achieved with AERF ink by exploiting the use of the LED apparatus positioned alongside the extruder head. By lowering the layer height and splitting the polymerization step it was possible to irradiate for a longer period the deposited ink achieving better object stability for the following post-curing. However, further developments are needed for the manufacturing of complex 3D models with the rCF inks.

**Table 3** Process parameters for 20D0B45RIVUF, 0D0B55GAMF and 0D6B20AERF inks

Material	Nozzle diameter [mm]	Layer height [mm]	Speed [mm/s]	Flow [%]
20D45RIVUF	1.6	0.4–0.5	10	130
0D55GAMF	1–1.5	0.25–0.75	8–12	100–105
6B20AERF	1	0.2	12–15	100

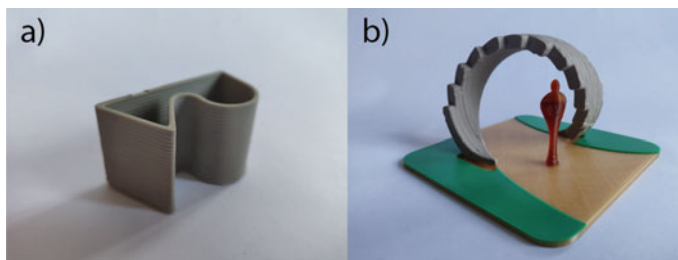


**Fig. 11** 3D printed structures with 20D45RIVUF ink: **a** test sample, **b** scale model of an arch



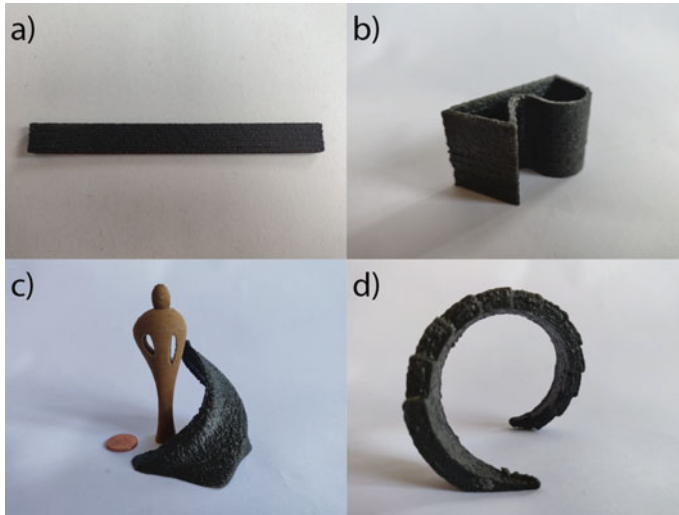


**Fig. 12** 3D printed structures with OD55GAMF ink: **a** tensile specimen, **b** test sample, **c** scale model of an arch, **d** scale model of a fountain

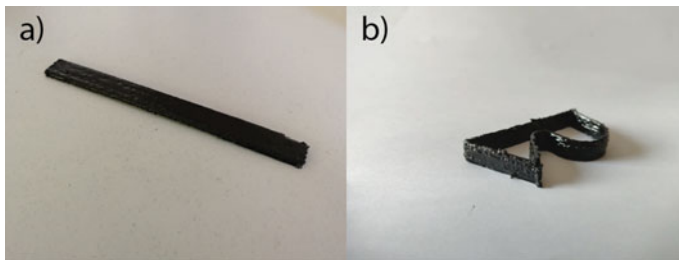


**Fig. 13** 3D printed structures with 6B20AERF ink: **a** tensile specimen, **b** test sample

Finally, some guidelines for UV-assisted LDM additive remanufacturing processes can be defined: crossing tool-paths are to be avoided using for example hexagonal infill; tilted surface up to  $30^\circ$  could be easily realized if the ink provides rapid enough photo-crosslinking. Spiral and Shell 3D Printing modes can be achieved easily, according to different geometrical shapes; layer height should be about  $\frac{1}{4}$  of the nozzle diameter: thicker layer height could result in less UV penetration and crosslinking. Printing speed is affected not only by viscosity but also by UV-conversion and cross-section geometries, for bigger areas it is necessary to increase the UV-irradiation time, decreasing the printing speed or splitting the deposition from the crosslinking step.

## 5.6 Mechanical Properties of Remanufactured Materials

Finally, the behavior of reprocessed composite material in terms of mechanical properties has been evaluated. The use of a recyclate material as reinforcement has an intrinsic limitation due to the recycling process which intrinsically reduces its reinforcement potential. The overall behavior is similar, and a brittle failure of the samples is observed for every 3D printed ink. Besides the outstanding stiffness reached by 6B20AERF, GAMF recyclate has shown good results compared to virgin GFs (Fig. 14).

The low performances of RIVUF recyclate were expected due to the poor amount of rGF in the final formulation, as reported in Table 4 equal to 5.4 wt%. Even though GAMF ink has a lower amount of reinforcement with respect to the virgin GF composite benchmark, the stiffness, and the overall mechanical behavior are comparable. The Halpin–Tsai model [46], shows a good prediction of the experimental values, demonstrating the quality of the evaluation through a large dataset of fibers measured with the Particle Analyzer MATLAB application [37]. A two-fold increase in modulus with respect to neat resin was measured for the 0D55GAMF formulation, and a three-fold increase was measured for 6B20AERF one as reported in Table 4.

Even though a lower elongation at break for the composite samples could be expected, SEM micrographs analysis evidenced the poor adhesion between fibers and matrix. For what concerns RIVUF ink, it was hard to find rGF at the fracture surface (Fig. 15a). The fracture surface of a 0D55GAMF specimen (Fig. 15b) shows indirectly the preferential alignment of the fibers after 3D printing. Most of the fibers are perpendicular to the fracture surface, consequently, the majority is aligned with the tensile test direction. During 3D printing, the strands of material were deposited parallelly to the tensile test direction, forcing the alignment of the fibers. This effect has been extensively studied in literature [18, 47]. Moreover, the detachment of the

**Fig. 14** Average mechanical behavior of additive remanufactured materials compared to neat resin behavior and virgin glass fiber 3D printed specimens

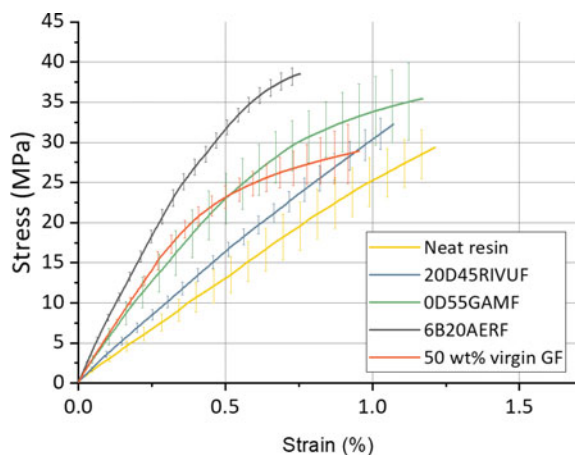


**Table 4** Average mechanical properties of additive remanufactured materials compared to neat resin behavior and virgin glass fiber 3D printed specimens

Material	Content of reinforcement [wt%]	Halpin–tsai elastic modulus [GPa]	Elastic modulus [GPa]	Tensile strength [MPa]	Elongation at break [%]
Neat resin [26]	0	n.d	2.6 ± 0.3	30.0 ± 5.0	1.2 ± 0.3
50 wt% GF [26]	50	8.9 ± 2.2	6.1 ± 0.4	26.3 ± 1.7	0.8 ± 0.2
20D45RIVUF	5.4	3.4 ± 0.2	3.6 ± 0.3	26.4 ± 5.2	0.9 ± 0.2
0D55GAMF	38.5	5.5 ± 1.8	5.5 ± 1.0	33.6 ± 5.6	0.9 ± 0.2
6B20AERF	20	8.1 ± 2.0	8.1 ± 0.5	39.4 ± 2.1	0.9 ± 0.1

fibers from the matrix is shown in Fig. 15c. Finally the fracture surfaces of 6B20AERF specimen exhibit similar conditions to GAMF specimen. As shown in Fig. 15d the detachment of the fibers from the matrix is not clear. Nevertheless, the tensile test results indicate a low adhesion between them.

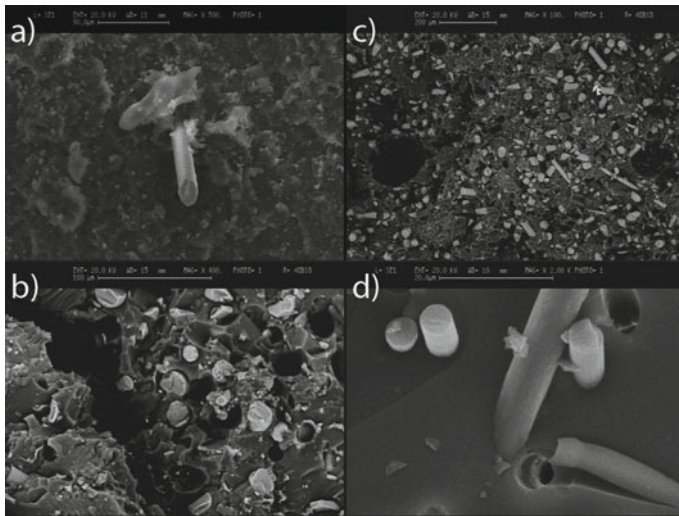


**Fig. 15** SEM micrograph of the fracture surface of tensile test specimens: **a** 20D45RIVUF, **b** and **c** 0D55GAMF, **d** 6B20AERF. Fibers aligned perpendicularly to the section are visible in the micrographs

## 6 Towards Urban Furniture and Large-Format Additive Manufacturing Concepts

### 6.1 *Urban Furniture from Recycled Plastics: A Case Study*

As previously discussed, an increasing quantity of wind blade turbines is going to be dismissed in the next few years. A noticeable amount of rGFRPs will be therefore available as a new raw reinforcement for remanufacturing processes. Considering also the properties of the above-mentioned 3D printable inks, other 3D printing apparatus should be taken into account, since “desktop-size” setups may limit the range of the potential applications.

Recently, the average size of the building volumes is increasing for industrial level 3D printers. This is primarily related to the rising demand for these printing volumes from the manufacturers, which are relying ever more on additive manufacturing processes. When the building volumes are equal or higher than 1 m<sup>3</sup>, the technology is better known as Large-Format Additive Manufacturing (LFAM). These technologies allow the processability of a wide range of materials, such as thermoplastics, composites, and ceramics [48, 49]. In its turn, extrusion-based LFAM is also known as Big Area Additive Manufacturing (BAAM) thanks to the gantry-based 3D printer developed at the Oak Ridge National Laboratory [50]. As an alternative, LFAM apparatus can also be based on other movement systems, such as 6-axis robotic arms.

Due to the possibility to directly construct big parts from a 3D model, the use of LFAM technology is spreading in those fields of applications with a high presence of handcrafted manufacturing processes and artisanal experiences, such as naval industry, construction, and furniture [51, 52]. A catamaran boat hull with an overall length of 10.36 m was successfully manufactured from a 3D printed mold made with CF-ABS and, very recently, a GF boat was entirely 3D printed with a 6-axis robot arm [53, 54]. As a matter of fact, the use of LFAM allows the reduction of times and costs for small batches of complex products.

Especially for the construction sector, the main innovation from LFAM is the chance to use new sustainable and efficient materials with a higher level of automation through the process [55]. From literature, many case studies range from high-performance concrete structures for construction to real buildings and homes [56, 57]. Furthermore, 3D printer manufacturers are focusing their attention on the development of new setups that allow the in situ production of architectural structures with sustainable raw materials, i.e. “Gaia” project from Wasp [58].

Similarly, furniture products were directly manufactured by using LFAM. Even if it is possible to produce artifacts for indoor spaces with these technologies [59], urban furniture represents a more interesting field of application, especially considering composite materials. The first 3D printed footpath bridge was opened to the public in 2016 (Madrid). Its main structure was made of a concrete powder reinforced with polypropylene fibers manufactured by means of a D-Shape printer developed

by Enrico Dini [60]. Thanks to a 6-axis robot arm, a metal footpath bridge was developed and 3D printed in Amsterdam (Fig. 16). Its overall length is 12.5 m, and the structure was inaugurated during the Dutch Design Week 2018 [61]. In both cases, the automation offered from the digitalization simplified the manufacturing process for the production of complex shapes. Other projects demonstrate the feasibility of urban furniture production from recycled materials, i.e. plastic. The custom-made chairs from “Moro Collection” (Studio Achoo) were 3D printed with plastic wastes from Belgium employing a large-scale 3D printer. They were developed for local-scale production in order to generate circular economy cases at the local level. A similar approach was followed by the “Print your City” project (The New Raw). In this case, the main goal was to raise awareness among citizens about the reuse of plastics by transforming wastes in street furniture. The project, firstly implemented only in Amsterdam (2016), was also carried out in Thessaloniki. The product collection is mainly composed of 3D printed tree pots and benches [62, 63]. Similar considerations could be made for theater and amusement park scenery parts. Their realization is limited to unique complex pieces, and the process is often material and time-consuming. In 2017, the first scenery for the Opera Theater in Rome was 3D printed with a DeltaWASP 3MT industrial 3D printer. Particularly, this 3D printed scenery could be easily recycled by shredding it and reusing the material for a new work [64].

In light of the above, urban furniture and amusement park elements seem the most suitable design application for LFAM with the 3D printable inks shown in this chapter. Accordingly, the products would be manufactured and post-processed in situ, reducing the environmental footprint related to supply chains [65]. Moreover, the final product could be produced avoiding molds and reducing the number of parts in assemblies. Two concepts were finally designed and 3D printed with the 3Drag LDM apparatus as a preliminary feasibility test [25, 66].



**Fig. 16** Metal footpath bridge from the Dutch Design Week 2018 [61]. Reprinted from Journal of Constructional Steel Research. 172, Gardner, L., Kyvelou, P., Herbert, G., Buchanan, C.: Testing and initial verification of the world’s first metal 3D printed bridge, 106,233 (2020), with permission from Elsevier

## 6.2 *Scaling-Up Challenges and Perspectives*

In order to develop the before-mentioned concepts, a scaling-up of the 3Drag LDM process should be carried out. Further work would be finalized not only to increase the building volumes but also to the improvement of the LDM process. Delta bot systems, due to the fixed build plate which transfers lower vibration to the 3D printed structure and their expandable construction, seem to be the best solution for the development of a large-format LDM 3D printer. Moreover, the moving structure of these systems can carry heavier tools and a bigger reservoir could be assembled to the extruder. Besides, the use of a screw extruder could be beneficial for the processing of a wider range of inks, the reduction of air bubbles entrapped in the material, and the prevention of the formation of aggregates.

## 7 **Conclusions and Future Research Perspectives**

In this work, an additive manufacturing process for rGFRP and rCF inks was developed at a desktop-scale according to LDM principles. At first, three essential remanufacturing requirements were detected to define the optimal formulations of the 3D printable inks.

RGFRPs and rCF recyclates were characterized to define their fiber content, granulometry, and morphology. Afterward, the ink formulations and the mixing technologies were determined to maximize the recycle content. Reactive diluent or rheological modifiers were added to the inks to increase the filler content or to better control the rheological behavior of the formulation. Furthermore, a proper curing cycle was defined to assure a good cross-linking degree of the inks.

The behavior of the 3D printable inks during the extrusion was predicted thanks to a systematic rheological characterization and the definition of an analysis that emulates the 3D printing process. To sum up, inks with a pseudoplastic behavior, rapid recovery of the deformation after the extrusion, and a quick fluid/solid-like transition are the most suitable materials, especially in case of incomplete UV cross-linking like for rCF.

Some representative geometries and design concepts were designed and 3D printed with the most performing ink formulation for each kind of recycle. In this way, structures with overhangs or complex geometries were successfully achieved. Despite its low reactivity, promising results were obtained with rCF ink thanks to a further modification of the 3D printer setup. Afterward, a shortlist of guidelines for the use of rGFRP and rCF inks with the developed 3D printing system was provided.

The mechanical behavior of these remanufactured materials was also investigated, and remarkable results were achieved. In particular, AER Fine samples demonstrated the high added value of rCF reprocessing even at low filler percentages.

At last, a focused analysis of Large-scale Additive Manufacturing was carried out to better define a possible field of application. Some considerations related to the

scale-up of the remanufacturing process were then mentioned identifying alternatives to the desktop system developed yet. Future research efforts should be targeted not only to the process scale-up but also on the exploration of different fields of applications as well as new matrix and filler systems.

## References

- Zindani, D., Kumar, K.: An insight into additive manufacturing of fiber reinforced polymer composite. *Int. J. Lightweight Mater. Manuf.* **2**, 267–278 (2019). <https://doi.org/10.1016/j.ijlmm.2019.08.004>
- Jiang, Z., Diggie, B., Tan, M.L., Viktorova, J., Bennett, C.W., Connal, L.A.: Extrusion 3D printing of polymeric materials with advanced properties. *Adv. Sci.* **7**, 2001379 (2020). <https://doi.org/10.1002/advs.202001379>
- Ali, Md.H., Batai, S., Sarbassov, D.: 3D printing: a critical review of current development and future prospects. *RPJ.* **25**, 1108–1126 (2019). <https://doi.org/10.1108/RPJ-11-2018-0293>
- Wang, Y., Zhou, Y., Lin, L., Corker, J., Fan, M.: Overview of 3D additive manufacturing (AM) and corresponding AM composites. *Compos. Part A: Appl. Sci. Manuf.* **139**, 106114 (2020). <https://doi.org/10.1016/j.compositesa.2020.106114>
- Kerns, J.: How 3D printing is changing auto manufacturing. <https://www.machinedesign.com/3d-printing-cad/article/21834982/how-3d-printing-is-changing-auto-manufacturing>
- McLaren website. <https://www.mclaren.com/racing/partners/stratasy/mclaren-deploys-stratasy-additive-manufacturing-improve-2017-car-performance/>. Last Accessed 28 Nov 2020
- Moi Composites homepage. <https://www.moi.am/>. Last Accessed 28 Nov 2020
- Markforged, Composite 3D Printing. <https://markforged.com/materials>. Last Accessed 28 Nov 2020
- Gately, R.D., Beirne, S., Latimer, G., Shirlaw, M., Kosasih, B., Warren, A., Steele, J.R., in het Panhuis, M.: Additive manufacturing, modeling and performance evaluation of 3D printed fins for surfboards. *MRS Adv.* **2**, 913–920 (2017). <https://doi.org/10.1557/adv.2017.107>
- Parandoush, P., Lin, D.: A review on additive manufacturing of polymer-fiber composites. *Compos. Struct.* **182**, 36–53 (2017). <https://doi.org/10.1016/j.compstruct.2017.08.088>
- Brenken, B., Barocio, E., Favaloro, A., Kunc, V., Pipes, R.B.: Fused filament fabrication of fiber-reinforced polymers: a review. *Addit. Manuf.* **21**, 1–16 (2018). <https://doi.org/10.1016/j.addma.2018.01.002>
- Deng, X., Zeng, Z., Peng, B., Yan, S., Ke, W.: Mechanical properties optimization of poly-ether-ether-ketone via fused deposition modeling. *Materials.* **11**, 216 (2018). <https://doi.org/10.3390/ma11020216>
- Cicala, G., Latteri, A., Del Curto, B., Lo Russo, A., Recca, G., Farè, S.: Engineering thermoplastics for additive manufacturing: a critical perspective with experimental evidence to support functional applications. *J. Appl. Biomater. Funct. Mater.* **15**, 10–18 (2017). <https://doi.org/10.5301/jabfm.5000343>
- Rahman, K.M., Letcher, T., Reese, R.: Mechanical properties of additively manufactured peek components using fused filament fabrication. In: Volume 2A: Advanced Manufacturing. p. V02AT02A009. American Society of Mechanical Engineers, Houston, Texas, USA (2015)
- Stoof, D., Pickering, K.: Sustainable composite fused deposition modelling filament using recycled pre-consumer polypropylene. *Compos. B Eng.* **135**, 110–118 (2018). <https://doi.org/10.1016/j.compositesb.2017.10.005>
- Le Duigou, A., Castro, M., Bevan, R., Martin, N.: 3D printing of wood fibre biocomposites: from mechanical to actuation functionality. *Mater. Des.* **96**, 106–114 (2016). <https://doi.org/10.1016/j.matdes.2016.02.018>

17. Blok, L.G., Longana, M.L., Yu, H., Woods, B.K.S.: An investigation into 3D printing of fibre reinforced thermoplastic composites. *Addit. Manuf.* **22**, 176–186 (2018). <https://doi.org/10.1016/j.addma.2018.04.039>
18. Compton, B.G., Lewis, J.A.: 3D-printing of lightweight cellular composites. *Adv. Mater.* **26**, 5930–5935 (2014). <https://doi.org/10.1002/adma.201401804>
19. Raney, J.R., Compton, B.G., Mueller, J., Ober, T.J., Shea, K., Lewis, J.A.: Rotational 3D printing of damage-tolerant composites with programmable mechanics. *Proc. Natl. Acad. Sci. USA* **115**, 1198–1203 (2018). <https://doi.org/10.1073/pnas.1715157115>
20. Mahajan, C., Cormier, D.: 3D printing of carbon fiber composites with preferentially aligned fibers. In: Cetinkaya, S., Ryan, J.K. (eds.) *Proceeding of 2015 Industrial and Systems Engineering Research Conference*. Nashville, Tennessee (2015)
21. Lewicki, J.P., Rodriguez, J.N., Zhu, C., Worsley, M.A., Wu, A.S., Kanarska, Y., Horn, J.D., Duoss, E.B., Ortega, J.M., Elmer, W., Hensleigh, R., Fellini, R.A., King, M.J.: 3D-printing of meso-structurally ordered carbon fiber/polymer composites with unprecedented orthotropic physical properties. *Sci. Rep.* **7**, 43401 (2017). <https://doi.org/10.1038/srep43401>
22. Griffini, G., Invernizzi, M., Levi, M., Natale, G., Postiglione, G., Turri, S.: 3D-printable CFR polymer composites with dual-cure sequential IPNs. *Polymer* **91**, 174–179 (2016). <https://doi.org/10.1016/j.polymer.2016.03.048>
23. Invernizzi, M., Natale, G., Levi, M., Turri, S., Griffini, G.: UV-assisted 3D printing of glass and carbon fiber-reinforced dual-cure polymer composites. *Materials*. **9**, 583 (2016). <https://doi.org/10.3390/ma9070583>
24. Tian, X., Liu, T., Wang, Q., Dilmurat, A., Li, D., Ziegmann, G.: Recycling and remanufacturing of 3D printed continuous carbon fiber reinforced PLA composites. *J. Clean. Prod.* **142**, 1609–1618 (2017). <https://doi.org/10.1016/j.jclepro.2016.11.139>
25. Mantelli, A., Levi, M., Turri, S., Suriano, R.: Remanufacturing of end-of-life glass-fiber reinforced composites via UV-assisted 3D printing. *RPJ*. **26**, 981–992 (2019). <https://doi.org/10.1108/RPJ-01-2019-0011>
26. Romani, A., Mantelli, A., Suriano, R., Levi, M., Turri, S.: Additive re-manufacturing of mechanically recycled end-of-life glass fiber-reinforced polymers for value-added circular design. *Materials*. **13**, 3545 (2020). <https://doi.org/10.3390/ma13163545>
27. Mantelli, A.: Syringe extruder for 3Drag printer. (2020). <https://doi.org/10.5281/ZENODO.4283444>
28. Mantelli, A.: 3Drag printer custom firmware for Liquid Deposition Modeling mode. Zenodo (2020)
29. DI001LE dimmable electronic power supply, <https://tecnoswitch.com/prodotti/alimentatori-ali-mentatore-dimmerabile-e-dimmer-per-led/>. Last Accessed 28 Nov 2020
30. Chen, K., Kuang, X., Li, V., Kang, G., Qi, H.J.: Fabrication of tough epoxy with shape memory effects by UV-assisted direct-ink write printing. *Soft. Matter*. **14**, 1879–1886 (2018). <https://doi.org/10.1039/c7sm02362f>
31. Scott, P.J., Rau, D.A., Wen, J., Nguyen, M., Kasprzak, C.R., Williams, C.B., Long, T.E.: Polymer-inorganic hybrid colloids for ultraviolet-assisted direct ink write of polymer nanocomposites. *Addit. Manuf.* **35**, 101393 (2020). <https://doi.org/10.1016/j.addma.2020.101393>
32. Mantelli, A.: 3Drag UV curing add-on. (2020). <https://doi.org/10.5281/ZENODO.4298907>
33. Martanto, W., Baisch, S.M., Costner, E.A., Prausnitz, M.R., Smith, M.K.: Fluid dynamics in conically tapered microneedles. *AIChE J.* **51**, 1599–1607 (2005). <https://doi.org/10.1002/aic.10424>
34. Li, M., Tian, X., Schreyer, D.J., Chen, X.: Effect of needle geometry on flow rate and cell damage in the dispensing-based biofabrication process. *Biotechnol. Progress*. **27**, 1777–1784 (2011). <https://doi.org/10.1002/btpr.679>
35. Udofia, E.N., Zhou, W.: A guiding framework for microextrusion additive manufacturing. *J. Manuf. Sci. Eng.* **141**, 050801 (2019). <https://doi.org/10.1115/1.4042607>
36. Sun, H., Kim, Y., Kim, Y.C., Park, I.K., Suhr, J., Byun, D., Choi, H.R., Kuk, K., Baek, O.H., Jung, Y.K., Choi, H.J., Kim, K.J., Nam, J.D.: Self-standing and shape-memorable UV-curing epoxy polymers for three-dimensional (3D) continuous-filament printing. *J. Mater. Chem. C*. **6**, 2996–3003 (2018). <https://doi.org/10.1039/C7TC04873D>



37. Mantelli, A.: Particle analyzer. Zenodo (2020)
38. Sharp, K.V., Adrian, R.J.: On flow-blocking particle structures in microtubes. *Microfluid. Nanofluid.* **1**, 376–380 (2005). <https://doi.org/10.1007/s10404-005-0043-x>
39. Agbangla, G.C., Climent, É., Bacchin, P.: Numerical investigation of channel blockage by flowing microparticles. *Comput. Fluids* **94**, 69–83 (2014). <https://doi.org/10.1016/j.compfluid.2014.01.018>
40. Shahzad, K., D’Avino, G., Greco, F., Guido, S., Maffettone, P.L.: Numerical investigation of hard-gel microparticle suspension dynamics in microfluidic channels: aggregation/fragmentation phenomena, and incipient clogging. *Chem. Eng. J.* **303**, 202–216 (2016). <https://doi.org/10.1016/j.ccej.2016.05.134>
41. Beran, T., Mulholland, T., Henning, F., Rudolph, N., Osswald, T.A.: Nozzle clogging factors during fused filament fabrication of spherical particle filled polymers. *Addit. Manuf.* **23**, 206–214 (2018). <https://doi.org/10.1016/j.addma.2018.08.009>
42. Mantelli, A., Romani, A., Suriano, R., Levi, M., Turri, S.: Direct ink writing of recycled composites with complex shapes: process parameters and ink optimization. *Adv. Eng. Mater.* **23**, 2100116 (2021). <https://doi.org/10.1002/adem.202100116>
43. Agnoli, E., Ciapponi, R., Levi, M., Turri, S.: Additive manufacturing of geopolymers modified with microalgal biomass biofiller from wastewater treatment plants. *Materials*. **12**, 1004 (2019). <https://doi.org/10.3390/ma12071004>
44. Paul, E.L., Atiemo-Obeng, V.A., Kresta, S.M.: *Handbook of Industrial Mixing*. John Wiley & Sons Inc., Hoboken, NJ, USA (2003)
45. De Capua, V.: LDM—3D printable polymer ink filled with EoL glass fibre reinforced composites, <http://hdl.handle.net/10589/148913>. (2019)
46. Halpin, J.C., Kardos, J.L.: The Halpin-Tsai equations: a review. *Polym. Eng. Sci.* **16**, 344–352 (1976). <https://doi.org/10.1002/pen.760160512>
47. Shofner, M.L., Lozano, K., Rodríguez-Macías, F.J., Barrera, E.V.: Nanofiber-reinforced polymers prepared by fused deposition modeling. *J. Appl. Polym. Sci.* **89**, 3081–3090 (2003). <https://doi.org/10.1002/app.12496>
48. Nieto, D.M., Molina, S.I.: Large-format fused deposition additive manufacturing: a review. *Rapid Prototyping J.* (2019). <https://doi.org/10.1108/RPJ-05-2018-0126>
49. Al Jassmi, H., Al Najjar, F., Mourad, A.-H.I.: Large-scale 3D printing: the way forward. *IOP Conf. Ser.: Mater. Sci. Eng.* **324**, 012088 (2018). <https://doi.org/10.1088/1757-899X/324/1/012088>
50. Roschli, A., Gaul, K.T., Boulger, A.M., Post, B.K., Chesser, P.C., Love, L.J., Blue, F., Borish, M.: Designing for big area additive manufacturing. *Addit. Manuf.* **25**, 275–285 (2019). <https://doi.org/10.1016/j.addma.2018.11.006>
51. Moreno Nieto, D., Casal López, V., Molina, S.I.: Large-format polymeric pellet-based additive manufacturing for the naval industry. *Addit. Manuf.* **23**, 79–85 (2018). <https://doi.org/10.1016/j.addma.2018.07.012>
52. Naboni, R., Kunic, A.: Bone-inspired 3D printed structures for construction applications. *GT Projetos*. **14**, 111–124 (2019). <https://doi.org/10.11606/gtp.v14i1.148496>
53. Post, B.K., Chesser, P.C., Lind, R.F., Roschli, A., Love, L.J., Gaul, K.T., Sallas, M., Blue, F., Wu, S.: Using big area additive manufacturing to directly manufacture a boat hull mould using big area additive manufacturing to directly manufacture a boat hull mould. *Virtual Phys. Prototyping*. 2759. (2019). <https://doi.org/10.1080/17452759.2018.1532798>
54. Mambo Project—MOI Composites, <https://www.moi.am/projects/mambo>. Accessed 19 Nov 2020, Last Accessed 19 Nov 2020
55. Ghaffar, S.H.: Additive manufacturing technology and its implementation in construction as an eco-innovative solution. *Autom. Constr.* **11** (2018)
56. Gosselin, C., Duballet, R., Roux, P., Gaudillère, N., Dirrenberger, J., Morel, P.: Large-scale 3D printing of ultra-high performance concrete—a new processing route for architects and builders. *Mater. Des.* **100**, 102–109 (2016). <https://doi.org/10.1016/j.matdes.2016.03.097>
57. Paolini, A., Kollmannsberger, S., Rank, E.: Additive manufacturing in construction: a review on processes, applications, and digital planning methods. *Addit. Manuf.* **30**, 100894 (2019). <https://doi.org/10.1016/j.addma.2019.100894>

58. 3D Printing for sustainable living. <https://www.3dwasp.com/en/3d-printing-for-sustainable-living/>. Accessed 19 Nov 2020
59. Novak, J.I., O'Neill, J.: A design for additive manufacturing case study: fingerprint stool on a BigRep ONE. *RPJ*. **25**, 1069–1079 (2019). <https://doi.org/10.1108/RPJ-10-2018-0278>
60. Lowke, D., Dini, E., Perrot, A., Weger, D., Gehlen, C., Dillenburger, B.: Particle-bed 3D printing in concrete construction—possibilities and challenges. *Cem. Concr. Res.* **112**, 50–65 (2018). <https://doi.org/10.1016/j.cemconres.2018.05.018>
61. Gardner, L., Kyvelou, P., Herbert, G., Buchanan, C.: Testing and initial verification of the world's first metal 3D printed bridge. *J. Constr. Steel Res.* **172**, 106233 (2020). <https://doi.org/10.1016/j.jcsr.2020.106233>
62. Moro Collection. <https://www.achoo.be/blackbaboon?lang=en>. Accessed 19 Nov 2020
63. Print your City. <https://www.printyour.city/>. Accessed 19 Nov 2020
64. The First 3D Printed Scenography. <https://www.3dwasp.com/en/the-first-3d-printed-theatre-scenic-design/>. Accessed 19 Nov 2020
65. Despeisse, M., Baumers, M., Brown, P., Charnley, F., Ford, S.J., Garmulewicz, A., Knowles, S., Minshall, T.H.W., Mortara, L., Reed-Tsochas, F.P., Rowley, J.: Unlocking value for a circular economy through 3D printing: a research agenda. *Technol. Forecast. Soc. Chang.* **115**, 75–84 (2017). <https://doi.org/10.1016/j.techfore.2016.09.021>
66. Romani, A., Mantelli, A., Levi, M.: Circular design for value-added remanufactured end-of-life composite material via additive manufacturing technology. In: Segalàs, J., Lazzarini, B. (eds.) *Proceeding of 19th European Roundtable for Sustainable Consumption and Production. Circular Europe for Sustainability: Design, Production and Consumption*. pp. 491–512. Institute for Sustainability Science and Technology, Universitat Politècnica de Catalunya, Barcelona (2019)

**Open Access** This chapter is licensed under the terms of the Creative Commons Attribution 4.0 International License (<http://creativecommons.org/licenses/by/4.0/>), which permits use, sharing, adaptation, distribution and reproduction in any medium or format, as long as you give appropriate credit to the original author(s) and the source, provide a link to the Creative Commons license and indicate if changes were made.

The images or other third party material in this chapter are included in the chapter's Creative Commons license, unless indicated otherwise in a credit line to the material. If material is not included in the chapter's Creative Commons license and your intended use is not permitted by statutory regulation or exceeds the permitted use, you will need to obtain permission directly from the copyright holder.

